Electric Power Systems Research 140 (2016) 958–964

Contents lists available at ScienceDirect

Electric Power Systems Research

journal homepage: www.elsevier.com/locate/epsr

Optimum transmitted power spectral distribution for broadband power line communication systems considering electromagnetic emissions

Apostolos Milioudis*, Georgios Andreou, Dimitris Labridis

Department of Electrical and Computer Engineering, Power Systems Laboratory (PSL), Aristotle University of Thessaloniki (AUTH), P.O. Box 486, 54124, Greece

ARTICLE INFO

Article history:
Received 26 August 2015
Received in revised form 6 March 2016
Accepted 29 March 2016
Available online 27 April 2016

Keywords:
Broadband over power lines (BPL)
Channel capacity
Electromagnetic interference
Electromagnetic compatibility (EMC)
Overhead power lines
Power line communications (PLC)

ABSTRACT

The study prior to the installation of a power-line communication (PLC) system requires detailed knowledge of the channel properties, such as transfer function, noise levels, and channel capacity in order to assess the services that can be provided. The channel capacity is greatly affected by the transmitted power over the available frequency range. At the same time, the values of transmitted power determine the electromagnetic field magnitude to the vicinity of the system. The simultaneous operation of different systems which share parts of the same frequency range, in the context of smart grid communications, has to be regulated in order to avoid excessive interference scenarios. Therefore, an algorithm that calculates the optimum power allocation of the transmitted power for PLC systems is proposed. The algorithm takes into account the maximum permitted values of electric field emitted from the PLC system and determines the transmitted power. The proposed algorithm is implemented for several test cases, while the corresponding channel capacities are calculated. It is shown that the proposed scheme better exploits the available frequency range and the transmission margins.

1. Introduction

Economical feasible technologies, such as power line communication (PLC) systems can be used in order to serve the increasing necessity for data transfer. This technology utilizes the existing electrical power grid infrastructure, hence it does not require investments for backbone creation. Future power systems in the form of smart grids are expected to incorporate information and communication technology (ICT) in order to enhance their reliability, offering to PLC technology a major chance for large scale implementation [1–6]. Several proposed methods require data communication and PLC systems could be utilized to do so.

The design of power grids was conducted aiming to deliver electric power at very low frequencies. However, PLC technology can utilize frequencies up to several MHz. Also power grids extent to vast areas with numerous branches. For that reason PLC signals suffer from attenuation and multipath propagation, problems similar to those appearing in wireless communication systems [7–10]. This makes the rigorous investigation of several aspects prior to a PLC system installation necessary [11–18]. The data capacity of the PLC communication channels could determine PLC utilization levels, which mainly depends on the existing noise, the transmitted power, the available frequency range and the transfer function of the channel.

Focusing on the transmitted power, it is affected and determined by the parameters of the system and by the fact that several systems that make use of the same frequency range have to be able to operate, respectively. Hence, the transmitted power levels have to comply with rules ensuring electromagnetic compatibility (EMC). The operation of PLC devices must not create interference to other communication devices at their vicinity. The procedure to determine the effect of a PLC device operation to its vicinity includes the measurement of the associated electric field at specific distance from the system [19]. The measured values have to not exceed predetermined values that are specified by organizations responsible for EMC. Several organizations have suggested maximum values for electric field magnitude created by PLC systems. However, as of today there is no common adopted values. The existing suggestions come from either state services or other organizations from various countries, such as Germany, Norway, BBC & NATO and the FCC from USA [20]. Emissions produced by power lines and PLC system operation have attracted some research interest.

* Corresponding author.
E-mail address: amilioud@auth.gr (A. Milioudis).

http://dx.doi.org/10.1016/j.epsr.2016.03.047
0378-7796/

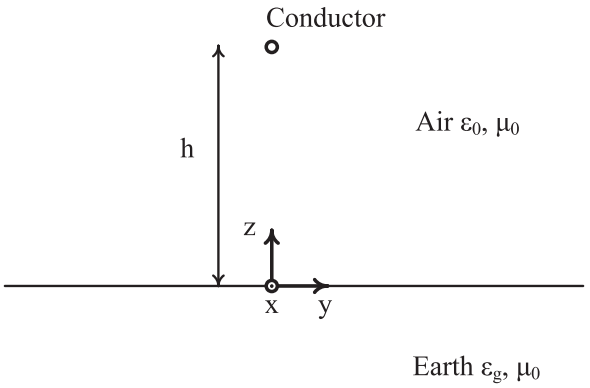

Fig. 1. Conductor at a height h from the surface of the earth.

In particular emission calculation methods have been investigated in [21–24]. However, the calculations of electromagnetic emissions were not used in order to optimize the overall transmitted power and hence the channel capacity. The channel capacity is highly affected by the overall transmitted power. Studies in the literature have adopted the water filling algorithm which prerequisites the overall transmitted power for the whole frequency range as an input and clearly do not take into account the limits for electromagnetic emissions [25–27]. Unlike this method, the proposed scheme takes into account electromagnetic emissions' limits in order to accurately compute the overall transmitted power.

In order to better exploit the available frequency range and permitted values for transmitted power, a new approach is presented. This approach takes into consideration all the parameters of a PLC arrangement installed in overhead MV networks. Furthermore, by adjusting the transmitted power for all available frequencies it fully exploits the available frequency range and at the same time does not exceed the predetermined values of emitted electric field in order to comply with EMC regulations. In Section 2 a theoretical formulation of the electric field emitted by a transmission line, both adopting a single and multiphase approach, is presented. Subsequently, Section 3 focuses on the theoretical approach regarding the electric field emitted by a broadband PLC system, while Section 4 presents the maximum allowed transmitted power calculation algorithm. All the conducted simulations are included in Section 5. Finally, the more important conclusions are shown in Section 6.

2. Electric field emitted by a transmission line

2.1. Single phase approach

Considering an overhead conductor at a height h from the surface of the ground, which carries current $Ie^{-\gamma x}$ with angular frequency ω, the electric field to the surrounding area can be calculated by making use of the electric and magnetic Hertz vectors [28], as suggested by Wait [29] for a thin conductor being at a distance from the line separating two mediums with different electromagnetic properties, which in the studied case are the air and the ground as shown in Fig. 1. Concretely, the dielectric constant and magnetic permeability of the air are ε_0, μ_0, respectively and the dielectric constant and magnetic permeability of the earth are ε_g, μ_0, respectively. The electric field per direction can be computed using electric and magnetic Hertz vectors as shown in Eqs. (1)–(3)

$$E_x(x,y,z) = \left(k_0^2 + \frac{\partial^2}{\partial x^2}\right)\Pi_E \tag{1}$$

$$E_y(x,y,z) = \frac{\partial^2 \Pi_E}{\partial y \partial x} + j\mu_0\omega\left(\frac{\partial \Pi_H}{\partial z}\right) \tag{2}$$

$$E_z(x,y,z) = \frac{\partial^2 \Pi_E}{\partial z \partial x} - j\mu_0\omega\left(\frac{\partial \Pi_H}{\partial y}\right) \tag{3}$$

where $k_0 = \omega\sqrt{\varepsilon_0\mu_0}$. Moreover, the electric and magnetic Hertz vector, Π_E Π_H, respectively, are defined as in Eqs. (4) and (5), respectively

$$\Pi_E = -\frac{j\mu_0\omega I}{4\pi k_0^2}\cdot e^{-\gamma x}\cdot \int_{-\infty}^{+\infty}\left[e^{u_0(z-h)} + R(\lambda)e^{-u_0(z+h)}\right]\cdot\frac{e^{-j\lambda y}}{u_0}d\lambda \tag{4}$$

$$\Pi_H = -\frac{j\mu_0\omega I}{4\pi k_0^2}\cdot e^{-\gamma x}\cdot \int_{-\infty}^{+\infty}\left[e^{-u_0 h} + M(\lambda)e^{-u_0 z}\right]\cdot\frac{e^{-j\lambda y}}{u_0}d\lambda. \tag{5}$$

Variable u_0 is computed using Eq. (6). Furthermore, functions $R(\lambda)$ and $M(\lambda)$ are defined using the boundary conditions on the mediums separating line and are given by Eqs. (7) and (8):

$$u_0 = \sqrt{\lambda^2 - \gamma^2 - k_0^2} \tag{6}$$

$$R(\lambda) = \frac{-\lambda^2\gamma^2(1-K)^2 + (\varepsilon_0\omega u_0 - \varepsilon_g\omega u_g K)(\mu_0\omega u_0 + \mu_0\omega u_g K)}{\lambda^2\gamma^2(1-K)^2 + (\varepsilon_0\omega u_0 + \varepsilon_g\omega u_g K)(\mu_0\omega u_0 + \mu_0\omega u_g K)} \tag{7}$$

$$M(\lambda) = \frac{2\lambda\gamma\varepsilon_0\omega u_0(1-K)}{\lambda^2\gamma^2(1-K)^2 + (\varepsilon_0\omega u_0 + \varepsilon_g\omega u_g K)(\mu_0\omega u_0 + \mu_0\omega u_g K)} \tag{8}$$

where $K = (k_0^2+\gamma^2)/(k_g^2+\gamma^2)$, $k_g = \omega\sqrt{\varepsilon_g\mu_0}$ and $u_g = \sqrt{\lambda^2 - \gamma^2 - k_g^2}$.

The analytical expressions for the components of electric field at each direction of the Cartesian coordinate system at a point with coordinates (x, y, z) are derived by using Eqs. (1)-(5) and Leibniz integral rule and are shown in Eqs. (9)-(11).

$$E_x(x,y,z) = (k_0^2+\gamma^2)\cdot\left(-\frac{j\mu_0\omega I}{4\pi k_0^2}\right)\cdot e^{-\gamma x} \cdot \int_{-\infty}^{+\infty}\left[e^{u_0(z-h)} + R(\lambda)e^{-u_0(z+h)}\right]\cdot\frac{e^{-j\lambda y}}{u_0}d\lambda \tag{9}$$

$$E_y(x,y,z) = \left(-\frac{j\mu_0\omega I\gamma}{4\pi k_0^2}\right)\cdot e^{-\gamma x} \cdot \int_{-\infty}^{+\infty}\left\{\left[e^{u_0(z-h)} + R(\lambda)e^{-u_0(z+h)}\right]\cdot j\lambda\cdot\frac{e^{-j\lambda y}}{u_0}\right\}d\lambda - \left(\frac{\mu_0^2\omega^2 I}{4\pi k_0^2}\right)\cdot e^{-\gamma x}\cdot\int_{-\infty}^{+\infty}\left[e^{-u_0 h}M(\lambda)u_0 e^{-u_0 z}\frac{e^{-j\lambda y}}{u_0}\right]d\lambda \tag{10}$$

$$E_z(x,y,z) = \left(\frac{j\mu_0\omega I\gamma}{4\pi k_0^2}\right)\cdot e^{-\gamma x} \cdot \int_{-\infty}^{+\infty}\left\{\left[u_0 e^{u_0(z-h)} - R(\lambda)u_0 e^{-u_0(z+h)}\right]\cdot\frac{e^{-j\lambda y}}{u_0}\right\}d\lambda + \left(\frac{\mu_0^2\omega^2 I}{4\pi k_0^2}\right)\cdot e^{-\gamma x}\cdot\int_{-\infty}^{+\infty}\left[e^{-u_0 h}M(\lambda)e^{-u_0 z}j\lambda\frac{e^{-j\lambda y}}{u_0}\right]d\lambda \tag{11}$$

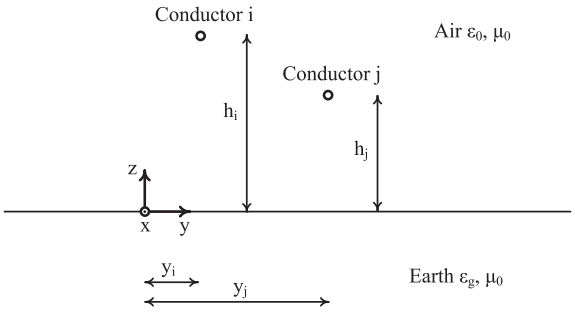

Fig. 2. Multiconductor configuration above ground.

2.2. Multiconductor approach

The single phase approach can be used for the computation of the electric field at the surrounding area of the conductor caused by the current that is carried. However, this approach has to be extended to take into account multiconductor arrangements.

Considering that the studied arrangement is illustrated in Fig. 2, and is comprised of N overhead conductors, each of which is at height h_i from the ground. The study of the equations providing the electric field for the single phase case gives that the propagation constant γ is considered known. For a multiconductor case the propagation constants are defined in the modal domain. Furthermore, the current carried by conductor i at some point x at the direction of the transmission line, $I_i(x)$, can be expressed using the modal currents as in Eq. (12).

$$I_i(x) = [\, T_I(i,1) \quad T_I(i,2) \quad \cdots \quad T_I(i,N)\,] \cdot \begin{bmatrix} I_{m1}(x) \\ I_{m2}(x) \\ \vdots \\ I_{mN}(x) \end{bmatrix} \tag{12}$$

The electric field emitted by conductor i of a multiconductor arrangement can be computed through the analysis of N single phase equivalents, each of which is defined by the propagation constant γ_{mj} and the current $T(i,j)\cdot I_{mj}(x)$, both corresponding to mode j [24]. Moreover, the coordinates of the conductor y_i and $z_i = h_i$ have to be used. More specifically, the electric field components created by the mode j of conductor i of a multiconductor configuration are defined in Eqs. (13)–(15).

$$E_{xij}(x,y,z) = (k_0^2 + \gamma_{mj}^2)\cdot \left[-\frac{j\mu_0\omega T_I(i,j) I_{mj}(x)}{4\pi k_0^2}\right] \cdot e^{-\gamma_{mj}x} \cdot \int_{-\infty}^{+\infty} [e^{u_0(z-h_i)} + R(\lambda)e^{-u_0(z+h_i)}] \cdot \frac{e^{-j\lambda(y-y_i)}}{u_0} d\lambda \tag{13}$$

$$E_{yij}(x,y,z) = \left[-\frac{j\mu_0\omega T_I(i,j) I_{mj}(x)\gamma_{mj}}{4\pi k_0^2}\right] \cdot e^{-\gamma_{mj}x} \cdot \int_{-\infty}^{+\infty} \left\{[e^{u_0(z-h_i)} + R(\lambda)e^{-u_0(z+h_i)}] \cdot j\lambda \cdot \frac{e^{-j\lambda(y-y_i)}}{u_0}\right\} d\lambda - \left[\frac{\mu_0^2\omega^2 T_I(i,j) I_{mj}(x)\gamma_{mj}}{4\pi k_0^2}\right] \cdot e^{-\gamma_{mj}x} \cdot \int_{-\infty}^{+\infty} \left[e^{-u_0 h_i} M(\lambda) u_0 e^{-u_0 z} \frac{e^{-j\lambda(y-y_i)}}{u_0}\right] d\lambda \tag{14}$$

$$E_{zij}(x,y,z) = \left[\frac{j\mu_0\omega T_I(i,j) I_{mj}(x)\gamma_{mj}}{4\pi k_0^2}\right] \cdot e^{-\gamma_{mi}x} \cdot \int_{-\infty}^{+\infty} \left\{[u_0 e^{u_0(z-h_i)} - R(\lambda)u_0 e^{-u_0(z+h_i)}] \cdot \frac{e^{-j\lambda(y-y_i)}}{u_0}\right\} d\lambda + \left[\frac{\mu_0^2\omega^2 T_I(i,j) I_{mj}(x)}{4\pi k_0^2}\right] \cdot e^{-\gamma_{mj}x} \cdot \int_{-\infty}^{+\infty} \left[e^{-u_0 h_i} M(\lambda) e^{-u_0 z} j\lambda \frac{e^{-j\lambda(y-y_i)}}{u_0}\right] d\lambda \tag{15}$$

Therefore, the total values of electric field components emitted by conductor i can be computed through Eqs. (16)-(18)

$$E_{xi}(x,y,z) = \sum_{j=1}^{N} E_{xij} \tag{16}$$

$$E_{yi}(x,y,z) = \sum_{j=1}^{N} E_{yij} \tag{17}$$

$$E_{zi}(x,y,z) = \sum_{j=1}^{N} E_{zij}. \tag{18}$$

Finally, the total values of the electric field components emitted by all conductors of the arrangement can be calculated by the sum of the values emitted by each conductor separately, as shown in Eqs. (19)–(21). The total rms value of the electric field at a point with (x, y, z) coordinates can be computed through Eq. (22)

$$E_x(x,y,z) = \sum_{i=1}^{N}\sum_{j=1}^{N} E_{xij} \tag{19}$$

$$E_y(x,y,z) = \sum_{i=1}^{N}\sum_{j=1}^{N} E_{yij} \tag{20}$$

$$E_z(x,y,z) = \sum_{i=1}^{N}\sum_{j=1}^{N} E_{zij} \tag{21}$$

$$E(x,y,z) = \sqrt{E_x^2(x,y,z) + E_y^2(x,y,z) + E_z^2(x,y,z)}. \tag{22}$$

3. Electric field emitted by a broadband PLC system

Electric field is generated at the surrounding area of a functioning overhead PLC system. Let us consider focusing on a part of the distribution network that does not contain branches and located between two installed PLC devices. Moreover, the first device, *Device 1*, is considered to be installed at point $x = 0$, functioning as data transmitter, while the second device, *Device 2*, is considered to be installed at point $x = L$, functioning as data receiver. The points of the installed devices are considered to be matched meaning that the input impedance matrix at the point $x = 0$ is equal to the characteristic impedance matrix of the multiconductor configuration as shown in (23) [30]

$$Z_{in} = Z_c. \tag{23}$$

The input current vector can be calculated using the known input impedance matrix $\mathbf{Z}_{in}$ and the input voltage vector of *Device 1* as shown in Eq. (24)

$$\mathbf{I}(0) = {Z_c}^{-1} V_{in}. \tag{24}$$

The transmission line matching at the installation point of *Device 2* ensures that there will not be reflected voltage and current waves, thus the maximum value of the phase currents will be measured at point $x = 0$ [30]. Hence, the maximum values of electric field are measured at yz plane intersecting the x axis at the same point. Conclusively, the calculated electric field values at this plane can be used within the context of a maximum transmitted power allocation procedure of an overhead PLC system.

4. Maximum allowed transmitted power calculation

The transmitted power can be computed, while knowing the voltage and current vectors at the *Device 1* installation point, as the real part of the complex power at the same point by using (25) [31]

$$\mathbf{P_{em}} = \frac{1}{2} \cdot Re(\mathbf{V_{in}}^{\mathbf{t}} \cdot \mathbf{I_0}^*) \tag{25}$$

where $Re(\cdot)$ denotes the real part operator.

The maximum allowed transmitted power can be associated to maximum values of electric field, as they are stated by several organizations and standards. Hence, the procedure to be adopted has to ensure that these maximum values will not be exceeded so as to comply with standards and organization suggestions and simultaneously that the available limits will be fully exploited. Therefore, a recursive procedure can be formulated through which the proper input voltage vector and eventually the maximum allowed transmitted power can be determined.

Algorithm 1. Maximum allowed transmitted power calculation $\mathbf{P}_{em}$.

1: Objective function to be minimized $E^{(k)} - E_{limit}$
2: Determine initial voltage vectors $\mathbf{V}_{in}{}^{(1)}$ and $\mathbf{V}_{in}{}^{(2)}$
3: Calculate corresponding input current vectors $\mathbf{I}_{in}{}^{(1)}$ and $\mathbf{I}_{in}{}^{(2)}$
4: Corresponding electric field values calculation $E^{(1)}$ and $E^{(2)}$ by using the procedure shown in Section 2.2
5: **repeat**
6: $\mathrm{V_{in}}^{(3)} = \mathrm{V_{in}}^{(2)} - [E^{(2)} - E_{limit}] \cdot \frac{\mathrm{V_{in}}^{(2)} - \mathrm{V_{in}}^{(1)}}{[E^{(2)} - E_{limit}] - [E^{(1)} - E_{limit}]}$
7: **if** $|E^{(1)} - E_{limit}| < |E^{(2)} - E_{limit}|$ **then**
8: $\mathbf{V}_{in}{}^{(2)} = \mathbf{V}_{in}{}^{(3)}$
9: **else**
10: $\mathbf{V}_{in}{}^{(1)} = \mathbf{V}_{in}{}^{(3)}$
11: **end if**
12: Calculate corresponding input current vector $\mathbf{I}_{in}{}^{(3)}$
13: Corresponding electric field value calculation $E^{(3)}$ by using the procedure shown in Section 2.2
14: **until** $|E^{(3)} - E_{limit}| < e$
15: $\mathbf{V}_{in} = \mathbf{V}_{in}{}^{(3)}$
16: $\mathbf{I_0} = \mathbf{Z}_{in}{}^{-1} \cdot \mathbf{V}_{in}$
17: $\mathrm{P_{em}} = \frac{1}{2} real(\mathrm{V_{in}}^{t} \cdot \mathrm{I_0}^*)$

Concretely, a recursive procedure with k repetitions is formulated and the difference among the calculated electric field value, E, and the value corresponding to the limit, E_{limit}, is the objective function to be minimized. Variable k corresponds to the number of repetitions needed for the algorithm to converge to the specified goal value. This process is adopted for each examined frequency that lies into the studied frequency range. For every input voltage vector $\mathbf{V}_{in}{}^{(k)}$ a corresponding current vector $\mathbf{I}_{in}{}^{(k)}$ can be calculated as well as the respective electric field value, $E^{(k)}$, at a specified point in the surrounding area of the studied arrangement. The purpose of the procedure is the derivation of the electric field value $E^{(k)}$ approaching the limit value E_{limit} within the range defined by the convergence criterion e. The algorithm initiation is held after choosing two random input voltage vectors $\mathbf{V}_{in}{}^{(1)}$ and $\mathbf{V}_{in}{}^{(2)}$, and the calculation of the corresponding input current vectors $\mathbf{I}_{in}{}^{(1)}$ and $\mathbf{I}_{in}{}^{(2)}$, as well as the electric field values $E^{(1)}$ and $E^{(2)}$ by using the procedure shown in Section 2.2, considering that the final solution does not lie among the initial input voltage choices. The proposed algorithm adopts an alternative approach to the root searching of non linear equation by linear interpolation and is presented thoroughly in Algorithm 1, the result of which is the vector $\mathbf{P}_{em}$ that complies with the studied limits of electric field caused by the function of a PLC system.

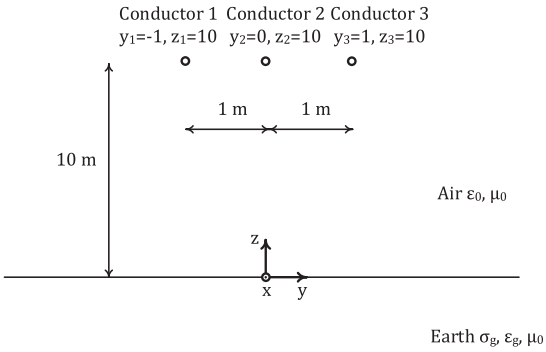

Fig. 3. Studied three-phase configuration.

5. Simulations

In order to develop a test case several parameters related to the studied arrangement, PLC system characteristics and EM activity at the vicinity have to be chosen. Specifically, the PLC system is considered to be installed at a three phase overhead MV distribution line with a distance of 1 km among two consecutive installed PLC devices. Furthermore, both communication devices are matched to the transmission line's characteristic impedance. The geometric configuration of the overhead MV transmission line comprises three ACSR phase wires of a 70/12 mm^2 cross section, located at a height of 10 m above the surface of the earth, in a symmetrical horizontal arrangement. Specifically, the outer conductors have 1 m spacing from the middle one, as shown in Fig. 3. The earth properties, considered for the simulations, correspond to conductivity equal to 0.01 S/m and relative permittivity equal to 10. Moreover, the studied external plane EM-field propagation forms a 40° angle with the x axis of the xz plane, and a 20° angle with the y axis of the xy plane. The directions of the Cartesian coordinate system are shown in Fig. 3. It is essential to clarify that all electric field calculations correspond to height equal to 1 m above the ground plane, i.e. $z = 1$, as in [19,20] if not stated otherwise. Moreover, the chosen generic amplitude of the examined EM field is considered to correspond equal to 0 dbμV/m for all examined frequencies [32]. Moreover, the convergence value e is chosen equal to 10^{-8}. It has to be stated that the per unit length electrical parameters of the studied arrangement was calculated using the model described in [33,34]. All simulation parameters are included in Table 1.

The way that the signal is injected can influence greatly the produced electric field to the vicinity of the line. Several signal injection methods can be implemented to the studied arrangement, which are shown in Table 2.

Table 1
Simulation parameters.

Conductor material	ACSR
Conductor cross section (mm^2)	70/12
Conductor height, h_i (m)	10
Distance among adjacent conductors (m)	1
Earth conductivity, σ_g (S/m)	0.01
Earth permittivity, ε_g (F/m)	$10 \cdot \varepsilon_0$
External field amplitude (dBμV/m)	0
External field angle with x axis of xz plane (°)	40
External field angle with y axis of xy plane (°)	20
Convergence criterion value, e	10^{-8}
Distance among PLC devices, L (m)	1000

Table 2
Signal injection types.

Parts used for signal injection	Code name
Conductor 1 and earth	A
Conductor 2 and earth	B
Conductor 3 and earth	C
Conductor 1 and conductor 2	D
Conductor 1 and conductor 3	E
Conductor 2 and conductor 3	F

Table 3
Different proposed emissions for PLC systems.

Organization	**F** (MHz)	EM_{lim}	D (m)
Germany	1–30	40–8.8 $\log f_{MHz}$ (dbμV/m)	3
Norway	1–30	20–7.7 $\log f_{MHz}$ (dbμA/m)	3
BBC & NATO	3–30	21.8-8.15 $\log f_{MHz}$ (dbμV/m)	1
FFC	1.705–30	30 (μV/m)	30

As stated there are several suggestions from different organizations regarding the maximum created electric field from a PLC system operation. These suggestions refer to the electric field magnitude at specific distance from the arrangement as shown in Table 3. Specifically, **F** corresponds to the frequency range associated to the maximum permitted electric field value determined by EM_{lim} at a distance specified by D.

The electric field components and the overall electric field calculated at a distance equal to 30 m from conductor 3 of the arrangement, while the signal injection is conducted between conductor 2 and the earth, i.e. signal injection type B, are illustrated versus frequency in Fig. 4. As shown the y component is the dominant and therefore the value of the overall electric field is mainly affected by that component. For that reason the respective values of E and E_y have a small deviation among them and the effect of frequency to their value follows similar patterns. It is worth mentioning that an electric field component at x axis is calculated. The x axis is parallel to the conductors. This shows that the propagation mode is not typically TEM (transverse electromagnetic), but quasi-TEM since the dominant component does not lie on the axis of the conductors. Moreover, the calculated values significantly exceeds the maximum allowed value from the FCC suggestion which is equal to 30 μV/m and is also the largest among all suggested values. Therefore, the value of the applied voltage, which is considered equal to 0.1 V has to be considerably adjusted in order to cope with suggested limitations.

The electric field components and the overall electric field are illustrated versus distance from the arrangement on the y axis as they are calculated at frequency equal to 5.5 MHz in Fig. 5. The B signal injection type is adopted. All components exhibit a symmetry with respect to $y = 0$ axis as expected, with maximum values

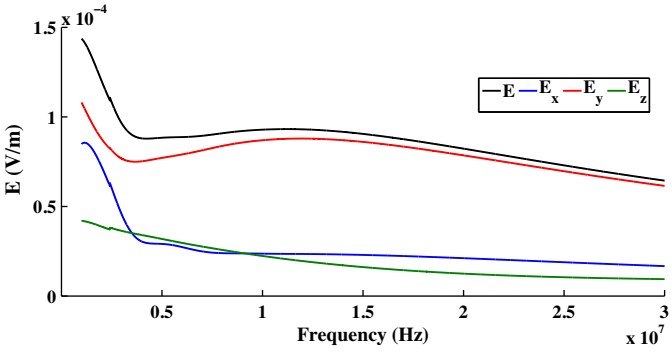

Fig. 4. Electric field components at a distance of 30 m from the arrangement versus frequency.

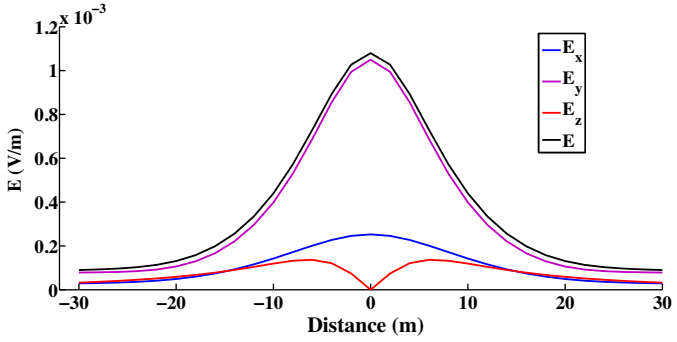

Fig. 5. Electric field components at frequency of 5.5 MHz versus distance from the arrangement.

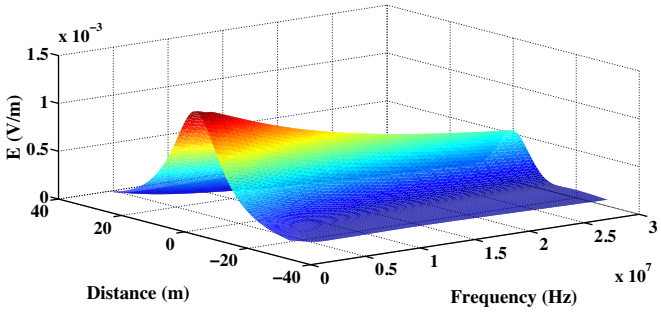

Fig. 6. Electric field versus frequency and distance from the arrangement.

for y and x components at the specific point, while z component is equal to zero. Similar to the previous case the applied voltage of 0.1 V leads to very high electric field values with respect to existing suggestions and has to be adjusted. The influence of frequency and distance from the middle conductor of the studied arrangement to the value of the overall electric field value is investigated in Fig. 6. Once more the signal injection type B is implemented and the used input voltage is equal to 0.1 V for all implemented frequencies, while the lateral distance varies from −30 to 30 m. The electric field values exhibit a symmetry with respect to the distance from the arrangement. Furthermore, the calculated values decrease while the used frequency increases. This happens because the input impedance value increases for higher frequencies thus leading to decreased input current values for steady input voltage.

The next studied case corresponds to the calculation of the maximum permitted transmission power versus frequency taking into account not to exceed the maximum values suggested by several organizations by implementing the proposed method. The calculations illustrated in Fig. 7 incorporate electric field value suggestions from FCC, Germany, Norway, BBC & NATO. The signal injection type B is used and the input voltage vector and therefore the transmitted

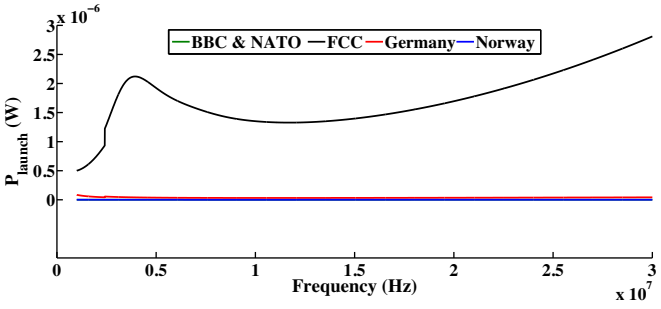

Fig. 7. Maximum transmitted power versus frequency.

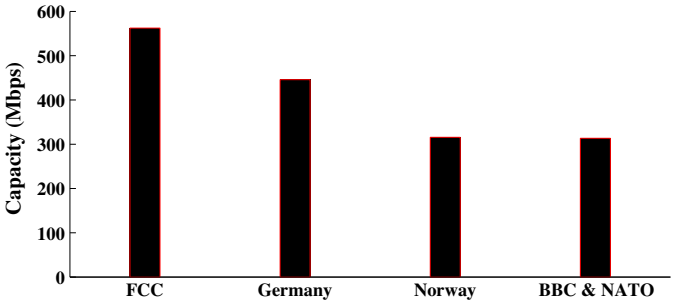

Fig. 8. Total capacity for maximum transmitted power of different proposals.

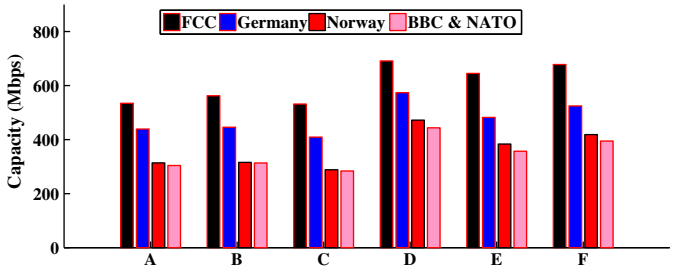

Fig. 9. Total capacity for maximum transmitted power of different proposals and different signal injections.

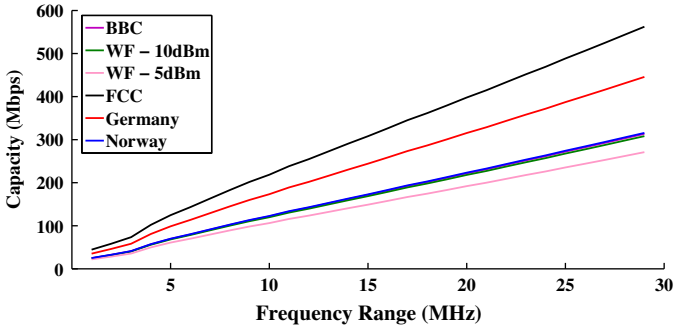

Fig. 10. Total capacity versus available bandwidth for different levels of injected power.

power are adjusted according to the calculated electric field value in order to comply with the various suggestions implementing the proposed algorithm. As shown in Fig. 7 the maximum permitted transmitted power corresponding to the FCC suggestion is significantly larger compared to all others. More concretely, second in magnitude is the curve corresponding to Germany suggestion followed by Norway and BBC & NATO suggestions. This is expected from the suggested maximum permitted electric field values shown in Table 3. Focusing on the curve for the FCC suggestion it is concluded that different transmitted power values are calculated for each studied frequency taking into account the specific characteristics of the studied arrangement.

The proposed scheme computes the optimum transmitted power for every frequency of the available frequency range complying with the limits of electromagnetic emissions. Therefore, the overall transmitted power results from the sum of all computed values for the available frequency range. However, studies from the literature have adopted a different approach [25–27]. Specifically, by implementing the water-filling algorithm for calculating the overall channel capacity similar studies required the overall transmitted power as an input of the method. This approach clearly does not take into account electromagnetic emissions limits in order to provide the overall transmitted power. Therefore, the advantage of the proposed scheme compared to existing studies in the literature is obvious.

The implementation of the proposed algorithm for the calculation of the maximum permitted transmitted power per used frequency affects the corresponding overall capacity of the communication channel on the physical layer. In Fig. 8 the computed overall capacity values in Mbps for signal injection type B and available frequency range with maximum frequency equal to 30 MHz are illustrated. The overall capacity for FCC suggestion approaches 600 Mbps, which is considered really high for broadband PLC systems in overhead MV lines. The capacity for Germany suggestion is 100 Mbps less than the previous case, while the values for Norway and BBC & NATO suggestions are quite similar and approximately 100 Mbps less than the capacity for Germany suggestion. Significant deviation among the various suggestions are derived. This makes the proposed method necessary and valuable tool for PLC systems design, in order to enhance electromagnetic compatibility.

The communication channel capacity corresponding to all possible signal injection types is studied in Fig. 9. It is derived that the cases of signal injection among one conductor and the earth (types A, B and C) correspond to lower capacity values in comparison with signal injection types incorporating two conductors (types D, E and F). This is due to the fact that for cases D, E and F the main circuit currents in some extent cancel each others created electric field. For that reason the maximum transmitted power levels are higher resulting to larger capacity values compared to signal injections using one conductor and the earth. The capacity for FCC suggestions and for cases D, E and F approach the value of 700 Mbps, which is considerably high taking into account that the maximum frequency of the available bandwidth is 30 MHz and similar study by Amirshahi et al. [25] calculated capacity close to 1 Gbps but for maximum frequency of the available frequency range equal to 100 MHz. Hence for smaller available frequency range but with the application of the proposed method the capacity is significantly enhanced.

In order to better illustrate the difference of the proposed scheme from the adopted techniques presented in the literature a comparison among the proposed scheme and the water filling (WF) algorithm is conducted. The calculated overall channel capacity versus frequency for the different maximum electric field suggestions using the proposed scheme and the water filling (WF) algorithm for different total transmitted power levels are shown in Fig. 10. The B signal type injection is adopted and the available maximum frequency is equal to 30 MHz. The WF algorithm takes as input the total transmitted power and distributes it over the whole available frequency range, whereas the proposed scheme calculated the maximum permitted transmitted power per used frequency in order not to exceed specific electric field value limits. By this way the proposed scheme exploits better the available frequency range. From Fig. 10 is deduced that the proposed method can be used to ensure electromagnetic compatibility while the WF algorithm implementation does not take it into account. It is illustrated that the WF algorithm with overall transmitted power equal to 5 dBm corresponds to the lower channel capacity values indicating that this value for overall transmitted power poorly exploits the available frequency range compared to every available suggestions, i.e. FCC, Germany, Norway and BBC & NATO.

6. Conclusion

In this paper a model which can be used to calculate the EM emissions from power lines and PLC systems is presented. Taking into account that the transmitted power of such systems has a significant impact in both the channel capacity and the interference induced on other systems utilizing the same frequency range a novel algorithm for optimum allocation is proposed. This algorithm

ensures that the available frequency range is fully exploited while at the same time the electric field values emitted by the system operation do not exceed prespecified values. The validity of the proposed model for emission calculations is verified by several simulations. The optimum transmitted power allocation algorithm is implemented for several emission suggestions reported in the literature and the effects to corresponding channel capacity is illustrated. The proposed approach can be a useful tool towards final specification of strict emission limits by several competent organizations towards ensuring both large channel capacities and electromagnetic compatibility. Moreover, it could greatly help the investigation of extensive PLC technology implementation for smart grid communication handling. Furthermore, the proposed scheme is compared with other existing approaches for transmitted power allocation existing in literature, that do not take into account the emission limitations, and it is shown that its implementation can lead to significant increase of channel capacity which could improve quality of service. Conclusively, the approach proposed in the manuscript constitutes the first time to include emission level compliance of PLC systems to the way that the transmitted power is allocated in order to achieve full exploitation of the available bandwidth and EMC.

References

[1] S. Galli, A. Scaglione, Z. Wang, For the grid and through the grid: the role of power line communications in the smart grid, Proc. IEEE 99 (6) (2011) 998–1027., http://dx.doi.org/10.1109/JPROC.2011.2109670.

[2] N. Ginot, M. Mannah, C. Batard, M. Machmoum, Application of power line communication for data transmission over PWM network, IEEE Trans. Smart Grid 1 (2) (2010) 178–185, http://dx.doi.org/10.1109/TSG.2010.2053225.

[3] S.-G. Yoon, S. Jang, Y.-H. Kim, S. Bahk, Opportunistic routing for smart grid with power line communication access networks, IEEE Trans. Smart Grid 5 (1) (2014) 303–311, http://dx.doi.org/10.1109/TSG.2013.2279184.

[4] S. Barmada, A. Musolino, M. Raugi, R. Rizzo, M. Tucci, A wavelet based method for the analysis of impulsive noise due to switch commutations in power line communication (PLC) systems, IEEE Trans. Smart Grid 2 (1) (2011) 92–101, http://dx.doi.org/10.1109/TSG.2010.2099135.

[5] E. Bakhoum, S-parameters model for data communications over 3-phase transmission lines, IEEE Trans. Smart Grid 2 (4) (2011) 615–623, http://dx.doi.org/10.1109/TSG.2011.2168613.

[6] S. Canale, A. Di Giorgio, A. Lanna, A. Mercurio, M. Panfili, A. Pietrabissa, Optimal planning and routing in medium voltage powerline communications networks, IEEE Trans. Smart Grid 4 (2) (2013) 711–719, http://dx.doi.org/10.1109/TSG.2012.2212469.

[7] W. Chen, Home Networking Basis: Transmission Environments and Wired/Wireless Protocols, Prentice Hall, 2003.

[8] H. Ferreira, L. Lampe, J. Newbury, T. Swart, Power Line Communications: Theory and Applications for Narrowband and Broadband Communications Over Power Lines, Wiley, 2010.

[9] J. Anatory, N. Theethayi, Broadband Power Line Communications Systems: Theory and Applications, Wit Pr/Computational Mechanics, 2010.

[10] H. Hrasnica, A. Haidine, R. Lehnert, Broadband Powerline Communications Networks: Network Design, John Wiley & Sons Inc., 2004.

[11] P. Amirshahi, S. Navidpour, M. Kavehrad, Performance analysis of uncoded and coded OFDM broadband transmission over low voltage power-line channels with impulsive noise, IEEE Trans. Power Deliv. 21 (4) (2006) 1927–1934, http://dx.doi.org/10.1109/TPWRD.2006.877073.

[12] A. Lazaropoulos, P. Cottis, Transmission characteristics of overhead medium-voltage power-line communication channels, IEEE Trans. Power Deliv. 24 (3) (2009) 1164–1173, http://dx.doi.org/10.1109/TPWRD.2008.2008467.

[13] J. Anatory, N. Theethayi, On the efficacy of using ground return in the broadband power-line communications; a transmission-line analysis, IEEE Trans. Power Deliv. 23 (1) (2008) 132–139, http://dx.doi.org/10.1109/TPWRD.2007.910987.

[14] J. Anatory, N. Theethayi, R. Thottappillil, Power-line communication channel model for interconnected networks – Part II: Multiconductor system, IEEE Trans. Power Deliv. 24 (1) (2009) 124–128, http://dx.doi.org/10.1109/TPWRD.2008.2005681.

[15] J. Anatory, M.M. Kissaka, N.H. Mvungi, Channel model for broadband power-line communication, IEEE Trans. Power Deliv. 22 (1) (2007) 135–141, http://dx.doi.org/10.1109/TPWRD.2006.881597.

[16] J. Anatory, N. Theethayi, R. Thottappillil, Channel characterization for indoor power-line networks, IEEE Trans. Power Deliv. 24 (4) (2009) 1883–1888, http://dx.doi.org/10.1109/TPWRD.2009.2021044.

[17] T.A. Papadopoulos, A.I. Chrysochos, G.K. Papagiannis, Narrowband power line communication: medium voltage cable modeling and laboratory experimental results, Electr. Power Syst. Res. 102 (2013) 50–60, http://dx.doi.org/10.1016/j.epsr.2013.04.009.

[18] F.R. Sabino Jr., G. Machado, M. de Melo, L. de Medeiros, The influence of soil electrical parameters on the electric field due to power line communications: measurements of frequency-dependent soil parameters, Electr. Power Syst. Res. 111 (2014) 9–13, http://dx.doi.org/10.1016/j.epsr.2014.01.023.

[19] IEEE Standard for Power Line Communication Equipment-Electromagnetic Compatibility (EMC) Requirements-Testing and Measurement Methods, IEEE Std 1775-2010, 2011, pp. 1–66, http://dx.doi.org/10.1109/IEEESTD.2011.5682873.

[20] HF Interference, Procedures and Tools, Final Report of NATO RTO Information Systems Technology (IST) Panel Research Task Group IST-050/RTG-022 (or Research Task Group IST-050), 2007.

[21] S. Liu, L. Greenstein, Modeling and interference evaluation of overhead medium-voltage broadband power line (BPL) systems, in: Global Telecommunications Conf., 2007, GLOBECOM '07, IEEE, 2007, pp. 134–139, http://dx.doi.org/10.1109/GLOCOM.2007.33.

[22] S. Liu, L. Greenstein, Interference evaluation of overhead medium-voltage broadband power line systems, IEEE Trans. Electromagn. Compat. 52 (4) (2010) 866–877, http://dx.doi.org/10.1109/TEMC.2010.2075934.

[23] P. Henry, Interference characteristics of broadband power line communication systems using aerial medium voltage wires, IEEE Commun. Mag. 43 (4) (2005) 92–98, http://dx.doi.org/10.1109/MCOM.2005.1421910.

[24] M. D'Amore, M. Sarto, Electromagnetic field radiated from broadband signal transmission on power line carrier channels, IEEE Trans. Power Deliv. 12 (2) (1997) 624–631.

[25] P. Amirshahi, M. Kavehrad, High-frequency characteristics of overhead multiconductor power lines for broadband communications, IEEE J. Sel. Areas Commun. 24 (7) (2006) 1292–1303, http://dx.doi.org/10.1109/JSAC.2006.874399.

[26] J. Anatory, N. Theethayi, R. Thottappillil, M. Kissaka, N. Mvungi, Broadband power-line communications: the channel capacity analysis, IEEE Trans. Power Deliv. 23 (1) (2008) 164–170, http://dx.doi.org/10.1109/TPWRD.2007.911001.

[27] A. Lazaropoulos, P. Cottis, Capacity of overhead medium voltage power line communication channels, IEEE Trans. Power Deliv. 25 (2) (2010) 723–733, http://dx.doi.org/10.1109/TPWRD.2009.2034907.

[28] J. Wait, Electromagnetic radiation from cylindrical structures, NASA STI/Recon Technical Report A, vol. 89, 1988, pp. 36562.

[29] J. Wait, Theory of wave propagation along a thin wire parallel to an interface, Radio Sci. 7 (6) (1972) 675–679.

[30] C.R. Paul, Analysis of Multiconductor Transmission Lines, Wiley.com, 2008.

[31] D.M. Pozar, Microwave Engineering, Wiley.com, 2009.

[32] A. Milioudis, K. Syranidis, G. Andreou, D. Labridis, Modeling of medium-voltage power-line communication systems noise levels, IEEE Trans. Power Deliv. 28 (4) (2013) 2004–2013, http://dx.doi.org/10.1109/TPWRD.2013.2258408.

[33] M. D'Amore, M. Sarto, Simulation models of a dissipative transmission line above a lossy ground for a wide-frequency range. I. Single conductor configuration, IEEE Trans. Electromagn. Compat. 38 (2) (1996) 127–138, http://dx.doi.org/10.1109/15.494615.

[34] M. D'Amore, M. Sarto, Simulation models of a dissipative transmission line above a lossy ground for a wide-frequency range. II. Multiconductor configuration, IEEE Trans. Electromagn. Compat. 38 (2) (1996) 139–149, http://dx.doi.org/10.1109/15.494616.